Persistent Silylated Phosphoranyl Radicals. Application to Dynamic Nuclear Polarization

S. Marque,[†] Y. Berchadsky,[†] P. Bertrand,[‡] A. Fournel,[‡] and P. Tordo*[,†]

Laboratoire de Structure et Réactivité des Espèces Paramagnétiques, Université de Provence, CNRS-UMR 6517-case 521, Av. Escadrille Normandie-Niemen 13397 Marseille Cedex 20, France, and Unité de Bioenergétique et d'Ingénierie des Protéines CNRS, 31, chemin Joseph Aiguier, 13402 Marseille, Cedex 20, France

K. Lang,[§,||] M. Moussavi,[||] and E. Belorizky[⊥]

Société ARPE, 70 avenue des Martyrs, 38000 Grenoble, France, Centre d'Etude Nucléaire de Grenoble, Laboratoire d'Electronique, de Technologie et d'Instrumentation, DSYS, CSME, 17 rue des Martyrs 38054 Grenoble, Cedex 9, France, and Laboratoire de Spectrométrie Physique (CNRS-UMR-5588), Université Joseph Fourier, Grenoble 1, BP 87, 38402 Saint Martin d'Hères, Cedex, France

Received: April 2, 1997; In Final Form: May 20, 1997[⊗]

New phosphoranyl radicals $[(R_3SiO)_3POSiR'_3]^\bullet$ (R = R′ = Et, **1**, R = iPr, R′ = Et, **2**) were generated and studied by EPR, in both liquid and frozen *n*-hexane. **1** and **2** were shown to be very persistent (for **1**, $\tau_{1/2} \sim$ 50 min at 293 K), and their EPR isotropic spectrum is composed of a large doublet resulting from the phosphorus hyperfine coupling ($A_P \sim 2800$ MHz). The modulation of the anisotropic part of the hyperfine phosphorus coupling was shown to be the main relaxation mechanism contributing to the EPR line width. Its contribution was close to 98% at 230 K and decreased to 75% at 330 K. The contribution of the exchange coupling between two radicals was negligible at 230 K but reached 25% at 330 K. Radicals **1** and **2**, strongly influenced the T_1 of the solvent hydrogens, and in *n*-hexane at 273 K the efficiency factor of **2** was 0.55. Using this value and a model previously described for stable nitroxides, the maximum value of the low-field dynamic nuclear polarization factor of an *n*-hexane solution of **2** was found to be close to 23×10^3. This value is approximately 10 times higher than the value measured and calculated for the most efficient nitroxides currently used in low-field DNP experiments.

Introduction

The basic principle of dynamic nuclear polarization (DNP) in liquids[1] is the amplification of the NMR signal of nuclei (mainly protons) attached to solvent molecules. This amplification is obtained through the coupling of the nuclear spin system, with the electronic spin system of stable or at least highly persistent free radicals used as solutes. When the polarizing free radical exhibits a strong scalar hyperfine coupling with a low-spin nucleus, the signal enhancement can be particularly high.[2−5] On the other hand, the intensity of the DNP depends also on other factors, like the magnitude of the EPR line width ΔH_{EPR} and the efficiency factor *f*, which measures the influence of the unpaired electronic spin on the longitudinal relaxation time of the solvent nuclei.[15]N-labeled stable nitroxides are routinely used in low-field NMR magnetometers; however, the [15]N hyperfine coupling is small (≈56 MHz), thus limiting the sensitivity of the apparatus.

Most free radicals centered on phosphorus, because of their strong phosphorus hyperfine coupling, could be of great interest for DNP. Triarylphosphoniumyl radicals, $Ar_3P^{\bullet+}$, which have been the subject of previous studies,[6−8] were characterized by a large phosphorus hyperfine coupling constant, $A_P \approx 700$ MHz, whereas for the nitroxide radicals commonly used in DNP experiments, $A_N \approx 60$ MHz. However, solutions of persistent triarylphosphoniumyl radicals could be prepared only by electrochemical oxidation of triarylphosphines; but these solutions were not appropriate for DNP applications owing to the presence of the supporting electrolyte.

During the last 25 years, phosphoranyl radicals, $Y_4P^\bullet$ (Y = OR, NR2, SR), generated by reaction of free radicals with tervalent phosphorus compounds, have been widely studied,[9−12] and electron paramagnetic resonance spectroscopy (EPR) was shown[10] to be the most important technique for determining either their fragmentation pathway or their structural and stereochemical properties. It is now well established that phosphoranyl radicals usually adopt a trigonal bipyramid (TBP) geometry, the unpaired electron being described by a molecular orbital delocalized over the phosphorus atom and the apical ligands and containing a significant weight of the phosphorus 3s orbital.[9−12] The large contribution of the P3s orbital to the SOMO (singly occupied molecular orbital) results in a large phosphorus coupling (2200−3600 MHz), and if the ligands do not contribute to the hyperfine coupling pattern, a large doublet is the main feature of the liquid solution EPR spectrum of a TBP phosphoranyl radical. All the EPR characteristics of TBP phosphoranyl radicals suggest that these species might be particularly efficient for DNP. However, as reported in the literature, kinetics of decay of these radicals are very fast and most of them are very short lived. We have recently shown[13] that phosphoranyl radicals bearing four (trialkylsilyl)oxy ligands, $[(R_3SiO)_3POSiR'_3]^\bullet$, can be very persistent in solution, and we investigated their EPR features in order to estimate their potential in DNP applications. We report hereafter the EPR parameters of radicals **1** and **2** (Scheme 1), and we will discuss the different factors contributing to their EPR line width. Moreover, for an *n*-hexane solution of radical **2**, we will report

* Author to whom all correspondence should be addressed.
[†] Université de Provence.
[‡] Unité de Bioenergétique et d'Ingénierie des Protéines CNRS.
[§] Société ARPE.
[||] Centre d'Etude Nucléaire de Grenoble.
[⊥] Université Joseph Fourier.
[⊗] Abstract published in *Advance ACS Abstracts,* July 1, 1997.

S1089-5639(97)01154-7 CCC: $14.00

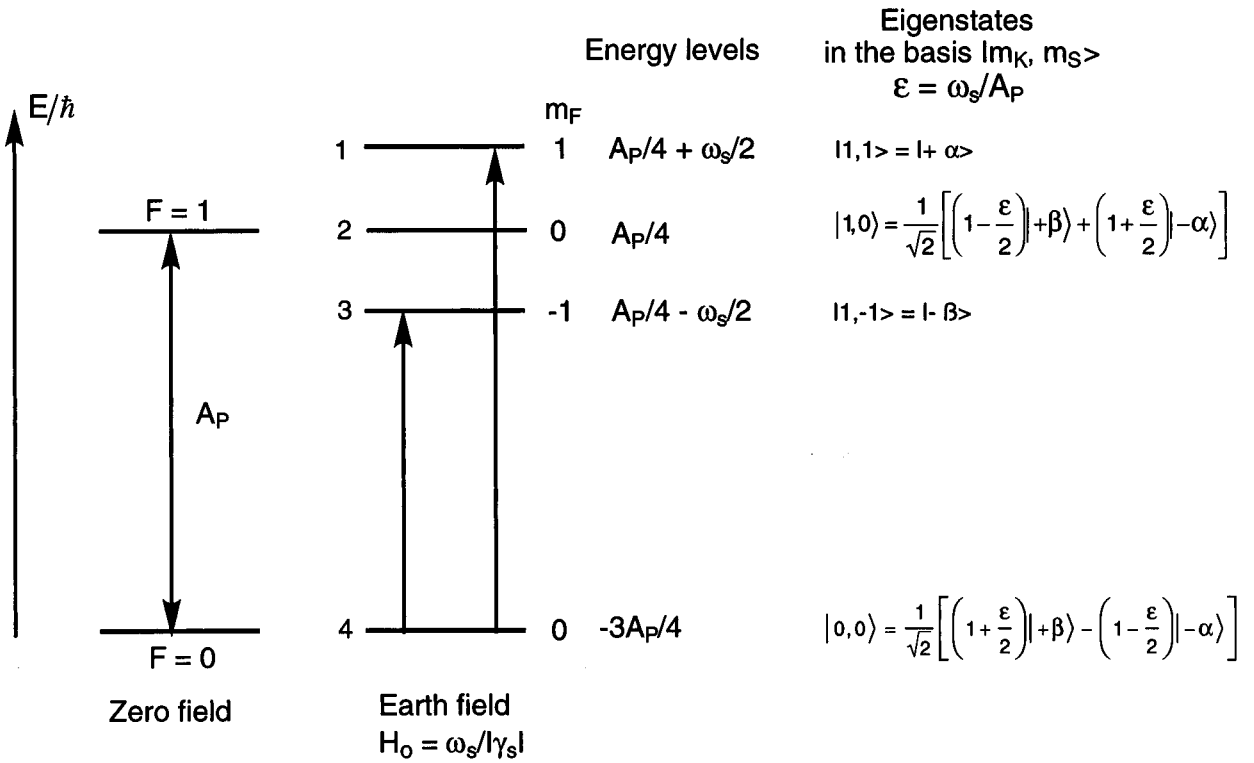

Figure 1. Energy levels and associated eigenstates corresponding to the spin hamiltonian for radicals **1** and **2** in a low magnetic field (the notations α, β stand for $m_S = +1/2$ and $-1/2$, respectively).

SCHEME 1

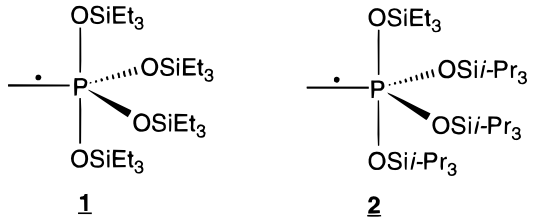

1 **2**

the measure of the efficiency factor *f* and the calculation of the DNP enhancement factor *F* for very low magnetic fields.

Theory

The coupling between the electronic spin system $\vec{S}$ and the proton solvent nuclear spin system $\vec{I}$ may be expressed as[3]

$$\langle I_z \rangle = I_0\left(1 - \rho f \frac{\langle S_z \rangle - S_0}{I_0}\right) \tag{1}$$

$\langle I_z \rangle$ and $\langle S_z \rangle$ are the nuclear and electronic polarizations, respectively, and I_0 and S_0 their values at thermal equilibrium. The factor ρ depends on the nature of the coupling between the two systems, either scalar ($\rho = -1$) and (or) dipolar ($\rho = 1/2$).[5] In the case of phosphoranyl radicals, we will assume that this coupling is purely dipolar, and we will use $\rho = 1/2$. The efficiency factor or leakage factor *f* depends both on the strength of the dipolar coupling and on the absence of other paramagnetic species in the solution; its value ranges between 0 and 1 and is given by

$$f = 1 - \frac{T_1}{T_{1,0}} \tag{2}$$

where T_1 and $T_{1,0}$ are the NMR longitudinal relaxation times of the solvent protons in the presence of the polarizing radical and for the pure solvent, respectively. The liquid phase EPR spectra of **1** and **2** are composed of a large doublet, resulting from the hyperfine scalar coupling A_P of the unpaired spin $\vec{S}$ with the spin $\vec{K}$ of the phosphorus nucleus. Neglecting the nuclear Zeeman interaction, the spin Hamiltonian can be written

$$\mathbf{H} = \hbar A_p \vec{S},\vec{K} + \mathbf{H}_{\text{Zeeman}} \tag{3}$$

where $\mathbf{H}_{\text{Zeeman}}$ represents the electronic Zeeman interaction. In very low magnetic fields (like the Earth's magnetic field), the hyperfine scalar coupling can be considered as the main part of the Hamiltonian and $\mathbf{H}_{\text{Zeeman}}$ as a small perturbation. The eigenfunctions of **H** and the corresponding energy levels were obtained using stationary perturbation theory and are shown in Figure 1.

It is interesting to point out that the energy level diagram for radicals **1** or **2** is the same as that of ^{15}N nitroxides commonly used for low-field DNP experiments.

For solutions of **1** or **2**, dynamic nuclear polarization could be induced by saturating either of the allowed transitions ($|0,0\rangle \leftrightarrow |1,1\rangle$(4 $\leftrightarrow$ 1) or $|0,0\rangle \leftrightarrow |1,-1\rangle$(4 3). The expected DNP enhancement factor *F* is then given by

$$F = \frac{\langle I_z \rangle}{I_0} \approx -\rho f \frac{\langle S_z \rangle}{I_0} \tag{4}$$

It is easy to show that in the absence of electron spin relaxation, the theoretical values of *F* would be given by

$$F_{14} = -\frac{1}{8}\frac{A_p}{\omega_I}\left(1 + \frac{3}{2}\frac{\omega_S}{A_p}\right)f \qquad F_{34} = -\frac{1}{8}\frac{A_p}{\omega_I}\left(1 - \frac{3}{2}\frac{\omega_S}{A_p}\right)f \tag{5}$$

where ω_S and ω_I are the electronic and nuclear angular Larmor frequencies respectively. The DNP enhancement factor has a lower value when the electron spin relaxation is considered. For this purpose, Ayant et al.[14,15] developed a model allowing calculation of the low-field DNP factor for solutions of ^{15}N

nitroxides. This model was recently improved by Belorizky et al.[16] and can be easily adapted to solutions of **1** or **2**. According to this model the DNP factor F can be expressed in a simplified form as

$$F = -\frac{A_p f}{2\omega_I}\Phi(\omega_s,\omega_1,\omega,A_p,\Delta H_{RPE}) \quad (6)$$

ΔH_{RPE} is the EPR line width at low field, and Φ is a complex function involving the complete electron spin relaxation matrix[16] that describes the time evolution of the populations of the levels due to the relaxation processes, $\omega_S = |\gamma_S|H_0$, $\omega_1 = |\gamma_S|H_1$, H_0 and H_1 being the Earth's magnetic field and the radio-frequency field rotating at angular frequency ω.

According to eq 6, high DNP factors are expected with solutions of free radicals exhibiting a high isotropic hyperfine coupling, a small EPR line width, and a strong interaction with the solvent molecules. Typical values for nitroxide solutions are $A_N = 60$ MHz, $f = 0.7$, and $\Delta H_{EPR} = 1.4 \times 10^{-5}$ T.[20]

The contributions to the electron spin relaxation matrix can be estimated by studying the influence of different factors (solvent viscosity, temperature, radical concentration) on the EPR line width. The low-field EPR line width ΔH_{EPR} cannot be directly measured; however, it can be deduced from the line width ΔH^x measured at high fields.[14,15] For radicals **1** and **2**, we assumed that the high-field EPR line width arises mainly from two mechanisms: the modulation of the anisotropic part of the hyperfine coupling ΔH^x_{HF} and the exchange coupling between two radicals ΔH^x_{EXC}. ΔH^x may be written as

$$\Delta H^x = \Delta H^x_{HF} + \Delta H^x_{EXC} \quad (7)$$

For a paramagnetic molecule exhibiting an axial symmetry and a hyperfine coupling with a spin K nucleus, it was shown[17] that ΔH^x_{HF} can be written

$$\Delta H^x_{HF} = \frac{2}{\gamma_S\sqrt{3}}\tau_r(\alpha + \beta m_K + \gamma m_K^2) \quad (8)$$

with

$$\alpha = \frac{1}{40}(\Delta A)^2 + \frac{1}{45}(\Delta g\cdot\omega_S)^2 - \frac{1}{12}\Delta g\cdot\Delta A\cdot A \quad (8a)$$

$$\beta = \frac{4}{45}(\Delta A\cdot\Delta g\cdot\omega_S) - \frac{17}{180}(\Delta A)^2\left(\frac{A}{\omega_S}\right) \quad (8b)$$

$$\gamma = \frac{1}{45}(\Delta A)^2\left(\frac{A}{\omega_S}\right) + \frac{1}{18}(\Delta A)^2 + \frac{1}{90}\Delta g\cdot\Delta A\cdot A \quad (8c)$$

$\tau_r = 4(\pi\eta r_e^3)/(3kT)$ is the rotational correlation time, r_e is the effective radius of the paramagnetic molecule, η is the solvent viscosity, $\Delta A = A_{||} - A_\perp$, and $\Delta g = g_{||} - g_\perp$.

The exchange coupling can be modeled by the exchange integal J[18] between two radical molecules with different m_K values. Only two values are considered for J expressed in frequency units: zero for $r > r_0$ and a constant value for $b < r < r_0$, where r is the interspin distance, r_0 is the radius of an effective collision sphere, and b is the minimal distance of approach of the two diffusing radicals. Thus, for radicals **1** or **2** with $K = {}^1/_2$, ΔH^x_{EXC} may be written as

$$\Delta H^x_{EXC} = \frac{2}{\gamma_S\sqrt{3}}\frac{2}{3}\frac{r_0}{b^*}\frac{kT}{\eta}N_S\phi(u) \quad (9)$$

where b^* is an effective distance that can significantly differ from b and is defined from the relative diffusion constant of two radicals by $D = (kT)/(6\pi b^*\eta)$, $u = (1/r_0)(D/2J)^{1/2}$, and N_S is the density number of paramagnetic molecules. $\phi(u)$ is defined by

$$\phi(u) = 1 - \mathrm{Re}\left\{\frac{\lambda + \frac{u}{\xi}\tanh\left[(1-\lambda)\frac{\xi}{u}\right]}{1 + \frac{\lambda\xi}{u}\tanh\left[(1-\lambda)\frac{\xi}{u}\right]}\right\} \quad (10)$$

with

$$\xi = (i/2)^{1/2} \quad \text{and} \quad \lambda = b/r_0$$

Finally, setting $x = T/10^4\eta$ and introducing C_S, the radical concentration in mol·L^{-1}, we obtained

$$\Delta H^x = \frac{\alpha_{HF}}{x} + \alpha_{exc}xC_S\phi(P\sqrt{x}) \quad (11)$$

with, in SI units, $\alpha_{HF} = 2 \times 10^8\, r_e^3\, (\alpha + \beta m_K + \gamma m_K^2)$; $\alpha_{exc} = 36.35 \times 10^{-5}\, r_0/b^*$; $P = 1.2 \times 10^{-9}\, (r_0^2 b^* J)^{-1/2}$.

Experimental Section

EPR Spectra. The radicals **1** and **2** were generated by UV photolysis of *n*-hexane solutions containing $Et_3SiOOSiEt_3$ and $P(OSiEt_3)_3$ or $P(OSiiPr_3)_3$ respectively. The EPR spectra were obtained with an ESP 300 Bruker X band spectrometer, equiped with a HP 5350B frequency meter and a NMR Gauss meter. The temperature was controlled by an ER 4111 VT apparatus. Irradiation of the samples was done with a 1000 W Xe-Hg lamp, and the beam was focused with a suprasil lens. The samples were degassed by several freeze−pump−thaw cycles under high vacuum (10^{-5} Torr). To record the anisotropic spectra, the radicals **1** and **2** were generated in *n*-hexane solutions at room temperature, and then these solutions were shock-cooled in liquid nitrogen to form glasses.

Measure of the Efficiency Factor *f*. A flask containing $P(OSiiPr_3)_3$ (0.3 M, 16.5 g) and $Et_3SiOOSiEt_3$ (0.05 M, 0.78 g) in 60 mL of *n*-hexane (distilled over sodium - benzophenone) was prepared under inert atmosphere and was sealed under high vacuum. After 90 min of UV photolysis at room temperature, the concentration of **2** was estimated (by EPR) to be 5×10^{-4} mol L^{-1}, and the flask was kept at 277 K. At this temperature the half-life of **2** is 165 min.

Nuclear relaxation time measurements were performed in the ambient Earth's magnetic field, on a home-made relaxometer[20−21] placed in an amagnetic chamber regulated at 273 K. The sensor consisted of two coils containing two flasks, one filled with the sample to study and the other empty. The coils were connected in opposition to a differential amplifier in order to cancel the external magnetic disturbances. The solvent protons were first polarized by applying a strong magnetic field. Then, this field was switched off, and the longitudinal temporal decay of the created magnetization was measured. In a semilogarithmic scale the observed signal decay was a line of slope $1/T_2'$, where T_2' is the transverse relaxation time including all magnetic inhomogeneities. Several experiments were performed using different polarization times until the maximal magnetization was obtained. A plot of the magnetization *vs* the polarization time provided the T_1 values with a 10% accuracy.

Results and Discussion

EPR Spectra. The isotropic EPR parameters of **1** and **2** were characteristic of phosphoranyl radicals with a TBP structure.

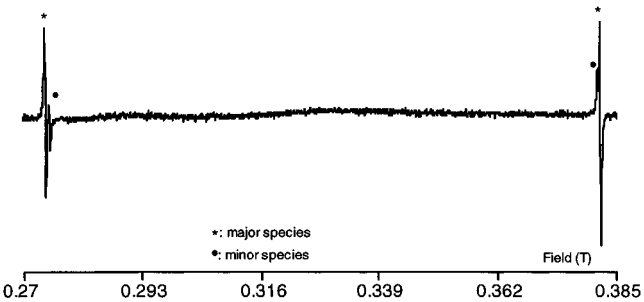

Figure 2. High-field isotropic EPR spectrum of **2a** (minor signal) and **2b** (major signal) in *n*-hexane at 253 K.

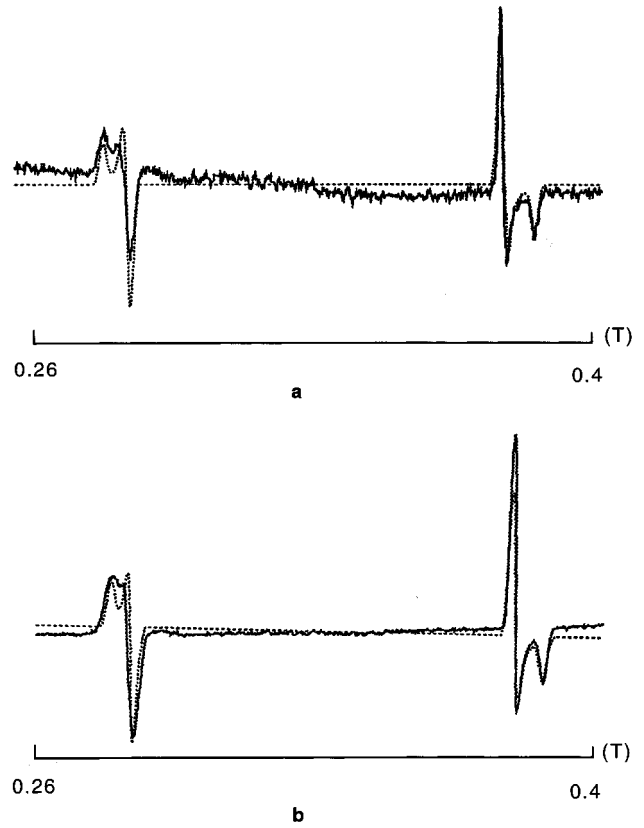

Figure 3. Experimental and calculated (dashed line) anisotropic spectra in frozen *n*-hexane (150 K): (a) radical **1**; (b) radical **2**.

SCHEME 2

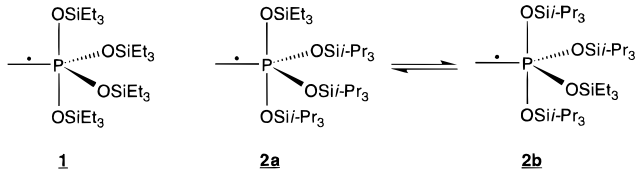

1 **2a** **2b**

It is important to mention that the EPR spectra of **2** clearly showed (Figure 2) the existence of an equilibrium between two pseudorotamers noted **2a** (minor component) and **2b** (Scheme 2).

A detailed description of the isotropic EPR spectra, as well as the EPR study of the kinetics of decay of **1** and **2**, will be published in a forthcoming paper.

The frozen solution spectra of **1** and **2** were studied to determine the diagonal components of the $\tilde{\mathbf{A}}$ and $\tilde{\mathbf{g}}$ tensors. Due to the very large phosphorus coupling, the spin Hamiltonian parameters cannot be deduced from a simple analysis based on perturbation theory.[19] A numerical simulation based on the full diagonalization of the Hamiltonian is needed. In these simulations[22] the axes of the $\tilde{\mathbf{A}}$ and $\tilde{\mathbf{g}}$ tensors were assumed to be parallel. The resonance field values, the eigenfunctions, and the transition probabilities corresponding to the spin Hamiltonian $\mathbf{H} = \beta\vec{B}\tilde{\mathbf{g}}\vec{S} + \vec{S}\tilde{\mathbf{A}}\vec{K}$ were determined. The spectral line width was obtained by assuming a uniform distribution of the orientations of the radical molecules and a convolution with a Gaussian distibution of the energy transitions characterized by a second moment[23] σ^2. The experimental and calculated spectra are shown in Figure 3a,b, and the values of the spin Hamiltonian parameters are listed in Table 1.

TABLE 1: EPR Characteristics of Radicals 1 and 2 Deduced from Their Anisotropic Spectra

radical	**1**	**2**
$A_{\|\|}$ (T)	0.1091 T 3055 MHz	0.1127 T 3156 MHz
$A_{\perp}$ (T)	0.0932 T 2610 MHz	0.0978 T 2738 MHz
A_p^{calc} (T) $= (A_{\|\|} + 2A_{\perp})/3$[a]	0.0985 T 2758 MHz	0.1027 T 2876 MHz
$g_{\|\|}$	2.001	2.0002
$g_{\perp}$	1.9995	2.0003
$g_{calc} = (g_{\|\|} + 2g_{\perp})/3$	2.0010	2.0016
B_0 (T) $= (A_{\|\|} + A_{\perp})/3$[a]	0.0053	0.0050
ρ_{3s}[b]	0.20	0.22
ρ_{3p}[b]	0.407	0.38
ρ_{3p}/ρ_{3s}	1.97	1.75

[a] Calculated from anisotropic parameters obtained at 150 K. [b] ρ_{3s} and ρ_{3p} are the spin densities in 3s and 3p orbitals, respectively, calculated using $A_0 = 0.4752$ T, $B_0 = 0.013$ T. [24]

TABLE 2: Physical Constants of *n*-Hexane[a] Solutions of 1 and 2 in SI Units

solution	**1**	**2**[b]
A_P (T) at 273 K	0.0997	0.1050 [0.1037][c]
ΔA (T)	0.0159	0.0149[d]
Δg	0.0015	-0.0001[d]
$r_{radical}$ (m)[e]	7×10^{-10}	7×10^{-10}
r_e (m)	4.75×10^{-10}	5.8×10^{-10}
b (m)	11×10^{-10}	11×10^{-10}
r_0/b	1.2[g]	1.2
b^*/b	1.2	1.2
J (s^{-1})	2×10^{10}	2×10^{10}
C_S (mol·L^{-1})[f]	5×10^{-4}	5×10^{-4}

[a] The radius of hexane is 3.8×10^{-10} m. [b] The EPR parameters for **2a** are in square brackets. [c] Obtained by simulation with the program of Pr Rockenbauer.[25] [d] Average values. [e] Obtained by Molecular Mechanic calculations on hydridophosphoranes corresponding to **1**, **2a**, and **2b**. [f] Estimated by EPR. [g] r_e, r_0, and b are fitted values.

High-Field EPR Line Width. As already mentioned, the relaxation matrix of the electron spin is needed to calculate the DNP factor of a radical solution. To build up that matrix for radicals **1** and **2**, we modeled their high-field EPR line width ΔH^x, using eqs 6−11. The values of the parameters used in the calculations are listed in Table 2. The EPR parameter values were obtained from the isotropic or anisotropic EPR spectra of *n*-hexane solutions. The effective radius r_e, the distance r_0, b^*, and the value of J were adjusted to give the best fit with the experimental values of ΔH^x.

For all the studied radicals **1**, **2a**, and **2b**, the calculations gave close values for the low-field line ($m_K = {}^1/_2$) and for the high-field line ($m_K = -{}^1/_2$). The results for radical **2a**, in the temperature range 230−330 K, are shown in Figure 4.

The agreement between the experimental and calculated ΔH^x values is satisfactory over the whole temperature range. The plot *vs* temperature of the weight of the two line width contributions included in our model (eq 7) is shown on Figure 5 for the low-field line of radical **2a**.

Over the whole temperature range investigated, the main contribution arises from the modulation of the anisotropic part of the phosphorus hyperfine coupling, ΔH^x_{HF}. The contribu-

TABLE 3: Low-Field Efficiency Factor *f* of an *n*-Hexane Solution of 2 at 273 K and Comparison with Other Paramagnetic Solutions[21]

radicals	TANO D^{15N}	TANO D^{15N}	TANO D^{15N}	Tober	$Mes_3P^{\bullet+}$ [a]	**2**
solvents	THF	MeCN	*n*-hexane	THF	MeCN	*n*-hexane
$T_{1,0}$ (s)	13	19	9,8	13	14,5	8.05
T_1 (s)	4	5.5	5	5.7	7.5	≈4
f	0.7	0.71	0.49	0.56	0.5	≈0.55
C (mol·L^{-1})	10^{-3}	10^{-3}	10^{-3}	10^{-3}	2×10^{-3}	$\approx 5 \times 10^{-4}$

[a] Mes = 2,4,6-trimethylphenyl.

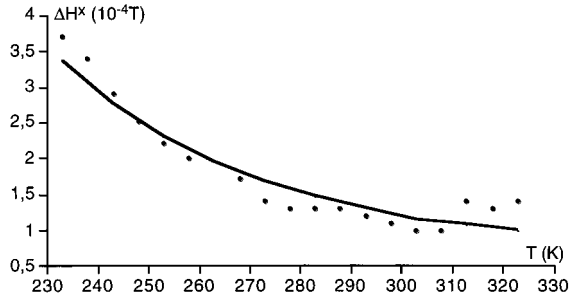

Figure 4. Temperature dependence of high-field EPR line width ΔH^x for radical **2a** ($m_k = {}^1/_2$): experimental (points), calculated (line).

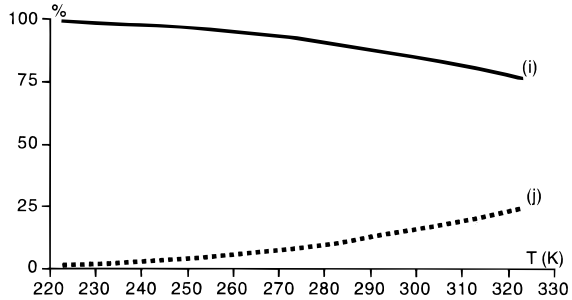

Figure 5. Temperature dependence of the different contributions ΔH^x_{HF} (i) and ΔH^x_{exc} (j) to the high-field EPR line width ΔH^x for **2a** ($m_k = {}^1/_2$).

tion of the exchange coupling, ΔH^x_{EXC}, is very small at low temperature, but it represents about 25% of the line width at temperatures higher than 330 K.

It should be noticed that we also modeled ΔH^x, including in eq 7 the spin-rotation coupling ΔH_{SR} and the dipolar coupling ΔH_{DIP}. The calculated curve was almost the same, the contributions of these two relaxation processes being lower than 1%. Note that from the value of the equilibrium constant of the **2a** ⇄ **2b** reaction, $K = 2.24$ at $T = 293$ K, we have for this temperature 70% of **2a** and 30% of **2b** species. We have checked that the presence of both pseudorotamers modifies the theoretical curve of Figure 4 by less than 1%.

Low-Field EPR Line Width. The low-field contributions to the EPR line width are deduced from the high-field contributions according to the following equations:[15]

$$\Delta H^x_{EXC} = \frac{3}{4}\Delta H^x_{HF} \qquad \Delta H_{HF} = \frac{2}{\gamma_S\sqrt{3}}\frac{1}{18}(\Delta A)^2\tau_r \quad (12)$$

A plot of $\Delta H_{EPR} = \Delta H_{EXC} + \Delta H_{HF}$ *vs* temperature for *n*-hexane solutions of radicals **1** and **2a** ($m_K = {}^1/_2$ line) is shown in Figure 6.

The values of ΔH_{EPR} for radicals **1** and **2a** are larger than the values found with solutions of ^{15}ND TANO [23] ($\Delta H_{EPR} = 0.12 \times 10^{-4}$ T at 293 K, for a radical concentration 5×10^{-4} mol·L^{-1}). For a 10^{-3} molar *n*-hexane solution of **2a**, we calculated $\Delta H_{EPR} = 0.3 \times 10^{-4}$ T at $T = 293$ K, while a lower value of 0.17×10^{-4} T was calculated in the same conditions for a solution of ^{15}ND TANO.[23] As shown below, the expected

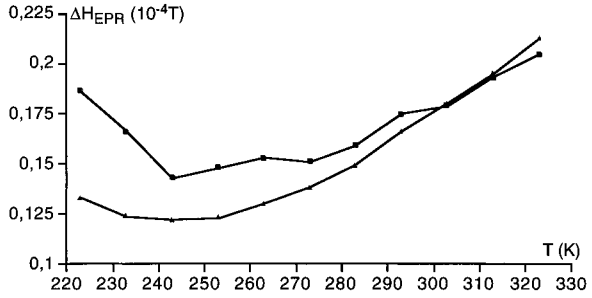

Figure 6. Calculated temperature dependence of the low-field EPR line widths for radical **1** (filled line) and **2a** (dashed line).

SCHEME 3

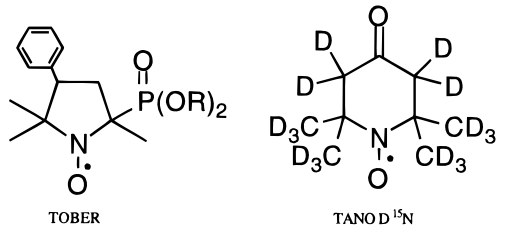

decrease of the DNP factor for solutions of radicals **1** or **2**, resulting from their larger EPR line width, is largely compensated by the huge difference in between the isotropic hyperfine couplings, $A_P \approx 0.1$ T for **1** or **2** and $A_N \approx 2 \times 10^{-3}$ T for ^{15}N-labeled nitroxides.

Efficiency Factor. The efficiency factor *f* is the last parameter needed to calculate the DNP factor *F*. The measured low-field longitudinal relaxation times $T_{1,0}$ and T_1 of the protons of pure *n*-hexane and of *n*-hexane solutions of **2**, respectively, are listed in Table 3. The efficiency factor *f* is given by eq 2, and its value is compararable with that of paramagnetic solutions previously used in DNP experiments.[16]**DNP Factor *F*.** Finally, using eq 6, which is completely derived in ref 16, we calculated the DNP enhancement factor for a *n*-hexane solution of **2a**, considering a radio-frequency excitation field, rotating at the angular frequency $A_P - \omega_S < \omega < A_P + \omega_S$. As the two EPR transitions are very close, they are simultaneously excitated and the excitation field is taken to give the best DNP enhancement factor for the $|0,0\rangle \leftrightarrow |1,1\rangle (4 \leftrightarrow 1)$ transition. The results are shown in Figure 7.

If the electron spin relaxation is not considered, the theoretical value of *F* according to eq 5 should be close to 10^5 for **2a** and 2.7×10^3 for ^{15}ND TANO. The higher value for **2a** is accounted for by the magnitude of the isotropic hyperfine constant A_p, which is nearly 47 times higher than A^{15}_N. However, when the electron spin relaxation was considered, the calculated *F* values were 23×10^3 and 2×10^3 for **2a** and ^{15}ND TANO, respectively. The important decrease observed for **2a** can be explained by the important contribution of the modulation of the hyperfine coupling to the EPR line width.

Conclusion

Owing to the steric crowding that hampers their dimerization and to the high Si−O bond dissociation energy that prevents

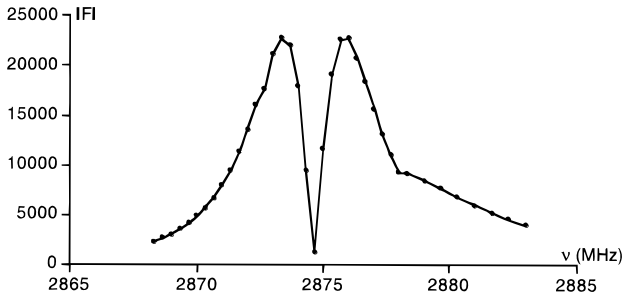

Figure 7. Calculated absolute values of the DNP factor F *vs* the frequency of the saturating radio-frequency field for radical **2**.

their fragmentation via a β-scission, the new phosphoranyl radicals **1** and **2** were shown to be very persistent in *n*-hexane solution. The large phosphorus couplings exhibited by **1** and **2** indicate an important contribution of the P3s valence orbital to their singly occupied molecular orbital (SOMO), in agreement with the small anisotropy (ΔA) of the phosphorus coupling. The modulation of the anisotropic part of the phosphorus coupling was shown to be the main electronic relaxation mechanism contributing to the EPR line width.

Radicals **1** and **2** strongly influenced the T_1 of the *n*-hexane protons, and at 293 K the efficiency factor of **2** was 0.55. Using this value and a model previously described for stable nitroxides, the maximum value of the low-field dynamic nuclear polarization factor of an *n*-hexane solution of **2a** was found to be close to 23×10^3. This value is approximately 10 times higher than the value measured and calculated for the most efficient nitroxides currently used in low-field DNP experiments like triglyme solutions of 1,1,3,3-tetramethymisoindol-*N*-oxyl (TMIO).

Acknowledgment. This work was supported by a grant from the Direction Générale des Armées (DGA-DRET). P.T. thanks Drs. K. U. Ingold and J. Lusztyk from the National Research Council of Canada for helpful discussions. Dr. A. Rockenbauer from the Technical University of Budapest is gratefully acknowledged for his comments and for providing his EPR simulation software.

References and Notes

(1) Abragam, A. *Phys. Rev.* **1955**, *98*, 1729.
(2) Abragam, A.; Combrisson, J.; Solomon, I. *C. R. Acad. Sci.* **1957**, 157.
(3) Solomon, I. *J. Phys. Radium* **1958**, *19*, 837.
(4) Landesman, A. *J. Phys. Radium* **1959**, *20*, 937.
(5) Müller-Warmuth, W.; Meise-Gresch, R. *Adv. Magn. Reson.* **1983**, *1*, 11.
(6) Ferroud-Plattet, M. P.; Belorizky, E.; Berchadsky, Y.; Tordo, P. *Ber. Besun-Ges Phys. Chem.* **1992**, *96*, 12.
(7) Palau, C. Thesis, l'Université de Provence, Marseille, France, 1992.
(8) Culcasi, M.; Berchadsky, Y.; Gronchi, G.; Tordo, P. *J. Org. Chem.* **1991**, *56*, 3537.
(9) Bentrude, W. G. In *The Chemistry of Organophosphorus Compounds*; Patai, S. series; Hartley, F. R., Ed.; John Wiley & Sons: Chichester, U.K., 1990; Vol. 1, p 541.
(10) Roberts, B. P. In *Advances in Free Radicals Chemistry*; Williams, G. H., Ed.; Heyden and Sons: London, 1980; Vol. 6, p 225.
(11) Bentrude, W. G. In *Reactive Intermediates*; Abramovitch, R. A., Ed.; Plenum Press: New York, 1983; Vol. 3, p 199.
(12) Bentrude, W. G. *Acc. Chem. Res.* **1982**, *15*, 117.
(13) Marque, S. Thesis, l'Université de d'Aix- Marseille 3, France, 1996.
(14) Ayant, Y.; Casalegno, R. *J. Phys.* **1978**, *39*, 325.
(15) Ayant, Y.; Besson, R.; Casalegno, R. *J. Phys.* **1980**, *41*, 1183.
(16) Lang, K.; Moussavi, M.; Belorizky, E. *J. Phys. Chem. A* **1997**, *101*, 1662.
(17) Wilson, R.; Kivelson, D. J. *J. Chem. Phys.* **1966**, *44*, 154.
(18) Ayant, Y.; *J. Phys.* **1976**, *37*, 219.
(19) Kerr, C. M. L.; Webster, K.; Williams, F. *J. Phys. Chem.* **1975**, *79*, 2650.
(20) Kernevez, N.; Duret, D.; Moussavi, M.; Léger, J. M. *IEEE Trans. Magn.* **1992**, *28*, 5.
(21) Ferroud-Plattet, M. P. Thesis, l'Université de Grenoble, 1992.
(22) Bertrand, P.; More, C.; Guigliarelli, B.; Fournel, A.; Bennet, B.; Howes, B. *J. Am. Chem. Soc.* **1994**, *116*, 3078.
(23) Ferroud-Plattet, M. P.; Ayant, Y.; Belorizky, E.; Tordo, P. *Solid State Comm.* **1991**, *80*, 947.
(24) Morton, J. R.; Preston, K. F. *J. Magn. Reson.* **1978**, *30*, 577.
(25) Rockenbauer, A.; Korecz, L. *Appl. Magn. Reson.* **1996**, *10*, 29.